HHS Public Access

Author manuscript

Nat Med. Author manuscript; available in PMC 2015 December 01.

Published in final edited form as:

Nat Med. 2015 June ; 21(6): 628–637. doi:10.1038/nm.3866.

KLF4 Dependent Phenotypic Modulation of SMCs Plays a Key Role in Atherosclerotic Plaque Pathogenesis

Laura S. Shankman[1,2], **Delphine Gomez**[1], **Olga A. Cherepanova**[1], **Morgan Salmon**[3], **Gabriel F. Alencar**[1,4], **Ryan M. Haskins**[1,5], **Pamela Swiatlowska**[1,6], **Alexandra A. C. Newman**[1,4], **Elizabeth S. Greene**[1], **Adam C. Straub**[7], **Brant Isakson**[1,2], **Gwendalyn J. Randolph**[8], and **Gary K. Owens**[1,2]

[1]Robert M. Berne Cardiovascular Research Center, University of Virginia, Charlottesville, VA, USA [2]Department of Molecular Physiology and Biological Physics, University of Virginia, Charlottesville, VA, USA [3]Department of Surgery, University of Virginia, Charlottesville, VA, USA [4]Department of Biochemistry and Molecular Genetics, University of Virginia, Charlottesville, VA, USA [5]Department of Pathology, University of Virginia, Charlottesville, VA, USA [6]Intercollegiate Faculty of Biotechnology, University of Gdansk, Gdansk, Poland [7]Department of Pharmacology and Chemical Biology, University of Pittsburgh, Pittsburgh, PA, USA [8]Division of Biology and Biomedical Sciences, Washington University, St. Louis, MO, USA

Abstract

Herein we employ *Myh11*-CreER^{T2} ROSA floxed STOP eYFP *Apoe*$^{-/-}$ smooth muscle cell (SMC) lineage tracing mice to show that traditional methods for detecting SMCs based on immuno-staining fail to detect > 80% of SMC-derived cells within advanced atherosclerotic lesions. These unidentified SMC-derived cells exhibit phenotypes of other cell lineages including macrophages (Mφs), and mesenchymal stem cells (MSCs). SMC-specific conditional knockout (KO) of Krüppel-like factor 4 (KLF4) resulted in reduced numbers of SMC-derived MSC-, and Mφ-like cells, marked reductions in lesion size, and increases in multiple indices of plaque stability, including an increase in fibrous cap thickness. Results of *in vivo* KLF4 ChIP-Seq

Correspondence should be addressed to Gary K. Owens, Ph.D. (gko@virginia.edu).

Contributions

L.S.S. conducted experiments, performed data analysis; generated most of the experimental mice; performed immunostaining, image analysis and flow cytometry; and was primary writer of the manuscript. D.G. performed *in vitro* ChIP analysis and conceived and performed all the ISH-PLA experiments. M.S. generated *Tagln* wild type lacZ *Apoe*$^{-/-}$, performed *in vivo* ChIP assays, performed immunohistochemistry, and data analysis. O.A.C. was involved in designing experiments and data analysis; assisted in image analysis, cell culture and animal experiments throughout the project. A.C.S. and B.I. participated in designing immuno-TEM protocol and analysis of images. R.M.H. optimized MSC staining IF protocols, conducted MSC differentiation experiments, and helped design cartoons. G.F.A. conducted data analysis of ChIP-seq experiments. P.S. assisted in cell culture experiments and analysis of data. A.A.C.N. peformed PDGFβR staining and analysis, E.S.G. assisted in animal experiments, conducted statistical analyses and performed immunohistochemistry and data analysis. L.S.S., D.G., M.S., O.A.C., E.S.G., B.I., G.J.R. and G.K.O. participated in making final manuscript revisions.

G.K.O. supervised the entire project and played a major role in experimental design, data interpretation, and writing the manuscript.

GEO accession number for KLF4 ChIP-seq data, GSE65812.

Competing financial interests

The authors declare no competing financial interests.

analyses, and studies in cultured SMC treated with cholesterol identified > 800 KLF4 target genes including many that regulate pro-inflammatory responses of SMC. Results indicate that the contribution of SMCs within atherosclerotic plaques has been greatly underestimated, and that KLF4-dependent transitions in SMC phenotype are critical in lesion pathogenesis.

Keywords

smooth muscle cell; krüppel-like factor 4; Mφ; phenotypic transitions; atherosclerosis; plaque pathogenesis

Introduction

Atherosclerosis is a disease of chronic inflammation and is the leading cause of morbidity and mortality worldwide. There is general consensus that the majority of coronary syndromes are the result of rupture of unstable plaques and associated thrombotic events[1-3]. Plaque instability has been associated with disruption of the fibrous cap, an atheroprotective layer of smooth muscle α-actin (ACTA2) positive cells that cover the atherosclerotic plaque[3-7]; large numbers of cells positive for Mφ markers such as LGALS3; and the presence of a large foam cell laden necrotic core within the plaque[2-4, 8]. Indeed, these data are interpreted as evidence that plaques which contain a high ratio of Mφs relative to SMCs are less stable, particularly those that have a thin ACTA2$^+$ fibrous cap presumed to be composed primarily of phenotypically modulated SMCs[9, 10].

Although ACTA2$^+$ and LGALS3$^+$ cells are assumed to be of SMC and myeloid lineage respectively, there is extensive ambiguity about cell lineage origin within atherosclerotic plaques[11]. These ambiguities were originally based on *in vitro* studies showing that SMCs down-regulate SMC markers and activate Mφ markers following cholesterol loading[12]; and that Mφs activate SMC genes following treatment with factors known to be present within lesions including thrombin[13]. However, the most compelling evidence that SMCs and Mφs are being misidentified within human advanced coronary lesions comes from studies of cross gender bone marrow transplant subjects showing that > 10% of ACTA2$^+$ cells within lesions are of hematopoietic stem cell (HSC) and not SMC origin[14]. Consistent with these human data, studies by Iwata et *al.*[15] demonstrated that a substantial fraction of cells within lesions of *Apoe*$^{-/-}$ mice that express SMC markers, including ACTA2 but not MYH11, are of HSC not SMC origin.

Conversely, there is also extensive evidence suggesting that many SMC-derived cells within advanced lesions of *Apoe*$^{-/-}$ mice lack detectible expression of conventional SMC markers like ACTA2 (ref. 16), and/or activate expression of Mφ markers[17]. This includes *in vivo* studies from our lab showing large numbers or ACTA2$^-$, MYH11$^-$, and TAGLN$^-$ cells within advanced lesions of *Apoe*$^{-/-}$ Western-diet fed mice that retain expression of a mutant *Tagln* lacZ transgene resistant to down-regulation compared to the wild type transgene[16]. Unfortunately, these studies are not definitive since we could not rule out the possibility that non-SMCs present within lesions may activate the mutant G/C repressor mutant *Tagln* lacZ transgene.

As such, despite decades of atherosclerosis research, we still do not know which cells within lesions are SMC-derived and to what extent they contribute to lesion pathogenesis. Recent studies by Feil et *al.*[17] using a *Tagln* ER^{T2}Cre LacZ SMC lineage tracing *Apoe*$^{-/-}$ mouse model provide evidence that SMC-derived cells within advanced lesions activate some Mφ markers including LGALS3 and CD68. Unfortunately, as highlighted in an editorial on this paper by Swirski et *al.*[18] the labeling efficiency of SMC in these studies was only 11%, precluding them from determining what fraction of Mφ-like cells within lesions are derived from SMC and most importantly, how these cells might contribute to lesion pathogenesis. A recent study[19] highlights the magnitude of the "SMC/Mφ mis-identification problem" with respect to understanding human disease in that they showed that 50% of foam cells within advanced human coronary artery lesions express the SMC marker ACTA2. However, the majority of these ACTA2^{+} foam cells also expressed the Mφ marker CD68 and represented 40% of all CD68^{+} lesion cells. Given clear evidence that Mφs can activate SMC markers and vice versa it is unclear if these cells are derived from SMCs, Mφs, or other cell type.

The preceding observations clearly establish that there is major ambiguity in identifying which cells within atherosclerotic lesions are SMC- versus Mφ-derived. However, in the final analysis, the most critical questions are: What regulates phenotypic transitions of SMCs, Mφs, and other cell types within lesions? What is the function of these cells? How do these phenotypic transitions impact overall disease pathogenesis? To begin to address these questions, we developed *Apoe*$^{-/-}$ mice where we could simultaneously lineage trace SMCs and study the effects of SMC-specific conditional KO of the stem cell pluripotency gene, KLF4, which we and others have previously shown plays a key role in regulating phenotypic transitions of SMC *in vivo* during development[20] and following carotid ligation injury[21], as well as *in vitro* in cultured SMCs treated with PDGFBB[22, 23], PDGFDD[24], and oxidized phospholipids[25].

Results

Most atherosclerotic plaque SMCs are not identified by ACTA2

SMCs are distinguished from other cell types by expression of a unique repertoire of genes including *Acta2*, *Tagln*, and *Myh11*, which are coordinately down-regulated, at least *in vitro*, during SMC phenotypic switching such that they may be undetectable using traditional immunohistochemical staining methods[11, 26]. Therefore, in order to rigorously analyze the overall contributions of SMCs to lesion pathogenesis, we utilized a *Myh11*-CreER^{T2} ROSA floxed STOP eYFP *Apoe*$^{-/-}$ (SMC YFP$^{+/+}$ *Apoe*$^{-/-}$) mouse model previously described[27] which labels > 95% of medial SMCs within large arteries (**Supplementary Fig. 1a**). To ensure the fidelity and SMC specificity of this lineage tracing model we completed a number of further validation studies beyond those shown in our previous studies[27] including showing: 1) SMC-specific YFP labeling within all tissue specimens examined with no detectable expression of the eYFP indicator gene in the absence of tamoxifen (**Supplementary Figs. 1a, 1b, and 2a**); 2) no detectable YFP^{+} cells within blood or bone marrow preparations based on flow cytometry (**Supplementary Fig. 2a**); 3) no evidence of YFP^{+} cells within lesions of Western diet fed SMC YFP$^{+/+}$ *Apoe*$^{-/-}$ mice not given tamoxifen (**Supplementary Fig. 2b**); 4) no detectable YFP+ cells in the blood of SMC

YFP$^{+/+}$ *Apoe*$^{-/-}$ mice given a high fat diet for 18 weeks (**Supplementary Fig. 2c**); and 5) YFP+ labeling of approximately 60% of freshly enzymatically dissociated cells from the ascending, descending thoracic aorta plus the abdominal aorta to the iliac bifurcation based on flow cytometry (**Supplementary Fig. 2d**). Since Cre excision is permanent, this SMC lineage tracing model system provides permanently lineage tagging of virtually all mature (MYH11^{+}) arterial SMCs that exist at the time of tamoxifen injection and subsequent determination of what they or their progeny become irrespective of continued expression of ACTA2, MYH11, or other SMC-marker genes.

We harvested brachiocephalic arteries (BCAs) from SMC YFP$^{+/+}$ *Apoe*$^{-/-}$ mice and immunostained them for YFP, ACTA2, and LGALS3 following 18 weeks of Western diet. Confocal microscopy z-stacks of the collected tissues were acquired and analyzed to accurately profile individual cells (**Fig. 1a-e**). Remarkably, ~82% of SMCs within atherosclerotic lesions (YFP^{+}DAPI^{+} cells) were ACTA2 negative (**Fig. 1a, Table 1**), indicating that the majority of SMCs within the lesion cannot be identified using traditional SMC markers. Results also showed that phenotypically modulated SMCs (YFP^{+}ACTA2^{-}/DAPI^{+}) comprised approximately 30% of the total cells within lesions (**Fig. 1a, Table 1**).

SMCs within atherosclerotic plaques express markers of Mϕs, MSCs, and MFs

When characterizing these phenotypically modulated SMCs we discovered YFP^{+} populations within lesions that expressed markers of Mφs (LGALS3) (**Fig. 1c**), MSCs (SCA1) (**Fig. 1d**), and MFs (ACTA2 and PDGFβR) (**Fig. 1e**). From this data we estimate the following distribution of SMC-derived cells within lesions: 30% Mφ-like (YFP^{+}ACTA2^{-}LGALS3^{+}); 7% MSC-like (YFP^{+}ACTA2^{-}SCA1^{+}); 12% MF-like (YFP^{+}ACTA2^{+}PDGFβR^{+}), 32–51% an unknown phenotype (YFP^{+}ACTA2^{-}LGALS3^{-}SCA1^{-}) (**Supplementary Table 1**). In addition, these analyses showed that 36% of LGALS3^{+} cells within advanced atherosclerotic lesions were YFP^{+}, indicating that ~1/3 of cells that would normally be classified as Mφs in most previous studies in the field originated from SMCs, not myeloid cells as previously assumed.

These initial studies were performed in paraffin embedded samples to maintain the ultrastructure of the plaque and to determine the location of various SMC-derived cells within lesions. However, this technique limits the number of simultaneous markers examined. To further characterize the various SMC phenotypes, we performed flow cytometric analyses of freshly dissociated cells from the aortic root through the iliac bifurcation. Results demonstrated that substantial numbers of SMC-derived cells express multiple additional Mφ/hematopoietic markers (**Fig. 1f**) including YFP^{+} cells that co-express ITGAM (CD11b) a monocyte/Mφ marker, and F4/80 a marker associated with mature Mφs, as well as the dendritic cell marker ITGAX (CD11c). In addition, flow cytometric analyses showed that 13% of SMCs were dual positive for the MSC markers SCA1 and ENG (CD105) (**Fig. 1f**). When analyzing YFP+ MSCs through traditional negative gating strategies (CD45^{-}CD34^{-}CDH5^{-}) we find that up to 45% of MSC-like cells within the aortas of 18 week Western diet fed SMC YFP$^{+/+}$ *Apoe*$^{-/-}$ mice are YFP+ (**Supplementary Fig. 3a**) although it is unclear if all of these are located within lesions or if they also contribute to adventitial SCA1+ cells previously described by several groups[28-32].

Gating strategies for all flow cytometry experiments were determined based on fluorescence minus one (FMO) controls (**Supplementary Fig. 3b, c**).

To further assess the morphological and possible functional properties of SMC derived Mφ-like cells *in vivo* we analyzed BCA lesions from SMC YFP$^{+/+}$ *Apoe*$^{-/-}$ mice by transmission electron microscopy combined with detection of YFP expression by immunogold labeling. As seen in **Fig. 2a** and **Supplementary Fig. 4**, we identified YFP^{+} cells containing multiple large lipid vacuoles that appear to be phagocytic. In addition, we flow sorted SMC-derived MSCs (YFP^{+}ENG^{+}SCA1^{+}), non-SMC derived MSCs (YFP^{-}ENG^{+}SCA1^{+}), and SMC non-MSCs (YFP^{+}ENG^{-}SCA1^{-}) from 18 week Western diet fed lineage tracing mice to test their ability to differentiate into multiple lineages including adipocytes and osteoblasts. After two passages in MSC maintenance media, the SMC non-MSCs became unhealthy and died (data not shown). The SMC-derived MSCs managed to survive in MSC maintenance media but appeared senescent and grew very slowly (**Fig. 2b**). They also failed to differentiate into either adipocytes (**Fig. 2c, d**) or osteoblasts (data not shown) when exposed to these respective differentiation medias. In contrast, the YFP^{-} (non-SMC-derived) MSCs grew well and showed high efficiency differentiation into adipocytes (**Fig. 2c, d**) and osteoblasts (data not shown). These data indicate that although a subset of SMC-derived cells within atherosclerotic lesions express multiple markers of MSCs, we have no evidence they are pluripotent and thus do not appear to function as MSCs.

SMCs within human atheromas express the Mϕ marker CD68

To independently detect phenotypically modulated SMCs that express LGALS3, and to validate a method for detecting these cells in human lesions, we utilized a novel *in situ* hybridization proximity ligation assay (ISH-PLA) recently developed by our lab[27]. This technique permits identification of phenotypically modulated SMCs within fixed tissues based on detection of H3K4dime of the *Myh11* promoter (PLA^{+}), a SMC-specific epigenetic signature that persists in cells that have no detectable expression of SMC markers[27, 33]. We first validated the method by showing that YFP^{+}LGALS3^{+} SMCs within our lineage tracing mice also retained this SMC-specific epigenetic signature (**Supplementary Fig. 5a**). We also showed that neither cultured RAW 264-7 mouse Mφ cells (**Supplementary Fig. 5b**) or human monocytes (**Supplementary Fig. 5c**) exhibited H3K4dime of *Myh11* when exposed to POVPC, an oxidative product of LDL that activates monocytes/Mφs[34].

To determine if SMC transition to a Mφ-like state in human lesions, we stained human coronary artery atherosclerotic lesions for CD68 and ACTA2 as well as ISH-PLA detection of the SMC-specific epigenetic marker *MYH11* H3K4dime. Multiple human coronary artery lesion sections from 12 human subjects were analyzed (**Supplementary Fig. 5d**). We found 18% of CD68^{+} cells with advanced coronary artery lesions in humans were positive for the SMC-specific *MYH11* H3K4dime epigenetic signature based on ISH-PLA assays (**Fig. 3a-c**), indicating that they were of SMC origin. To further validate these findings, we performed ISH-PLA analysis of *MYH11* H3K4dime in coronary artery samples from men that had received a cross gender heart transplant (**Supplementary Fig. 6**) and found *MYH11* H3K4dime PLA^{+} CD68^{+} cells that were Y-chromosome negative (**Fig. 3d**), consistent with these Mφ-like cells being of SMC and not hematopoietic origin. Importantly, we never saw

cells that were *MYH11* H3K4dime PLA$^+$ and Y-chromosome$^+$ (**Fig. 3d** and unpublished data) thus clearly demonstrating that myeloid cells do not acquire the *MYH11* H3K4diMe SMC epigenetic signature even in the context of human atherosclerotic lesions.

KLF4 plays a critical role in regulating SMC phenotype and overall plaque pathogenesis

We have previously shown that KLF4, an ESC and iPS cell pluripotency factor[35], is required for SMC phenotypic switching in several *in vitro*[25, 36] models. However, as yet there is no evidence that SMC phenotypic transitions within atherosclerotic lesions are KLF4 dependent, and if so, what role these transitions play in lesion pathogenesis.

Consistent with our hypothesis that KLF4 regulates phenotypic transitions of SMCs within atherosclerotic lesions, we observed large numbers of YFP$^+$ cells within BCA lesions from 18 week Western diet fed SMC YFP$^{+/+}$ *Apoe*$^{-/-}$ mice that expressed KLF4 (**Supplementary Fig. 7a**). To determine if KLF4 regulates SMC phenotypic transitions and overall lesion pathogenesis, we crossed the SMC YFP$^{+/+}$ *Apoe*$^{-/-}$ mouse with *Klf4*$^{FL/FL}$ mice. We observed highly efficacious recombination of the floxed *Klf4* alleles (*Klf4*$^{\Delta/\Delta}$) after tamoxifen treatment (**Supplementary Fig. 7b, c**) including what we estimate to be nearly 100% recombination within SMCs in the aorta when corrected for > 40% non-SMC DNA present in these samples based on flow cytometric evaluations (**Supplementary Fig. 2b**). After 18 weeks of Western diet feeding SMC YFP$^{+/+}$ *Klf4*$^{WT/WT}$ *Apoe*$^{-/-}$ and SMC YFP$^{+/+}$ *Klf4*$^{\Delta/\Delta}$ *Apoe*$^{-/-}$ mice (**Fig. 4a**) we determined that loss of *Klf4* exclusively in SMCs resulted in a nearly 50% reduction in lesion size (**Fig. 4b**) and multiple changes consistent with increased plaque stability including a > 2-fold increase in fibrous cap area (**Fig. 4c**), an increase in ACTA2$^+$ cells within the fibrous cap (**Fig. 4d**), and a reduced number of LGALS3$^+$ cells (**Fig. 4e**).

SMC lineage tracing analyses showed that loss of *Klf4* within SMCs did not result in a change in the overall number of SMCs (YFP$^+$ cells) within the lesions (**Supplementary Fig. 8a**), but resulted in major changes in SMC phenotypic transitions. This included a 53% decrease in the number of Mφ-like SMCs (YFP$^+$LGALS3$^+$/YFP$^+$) within the lesion (**Fig. 4e**), a 70% decrease in the MSC-like SMCs within the media underlying lesions (**Supplementary Fig. 8b**), but no change in the MSC-like SMCs in the lesion itself (**Supplementary Fig. 8c**). Consistent with these results, flow cytometric analyses showed a decrease in the total number of SMC-derived MSC-like cells (YFP$^+$SCA1$^+$ENG$^+$CDH5$^-$PTPRC$^-$CD34$^-$) (**Supplementary Fig. 8d**) but no change in either the total MSC population (**Supplementary Fig. 8e**) or the total number of YFP$^+$ cells (**Supplementary Fig. 8f**). SMC specific *Klf4* KO mice also showed an increase in the total number of ACTA2$^+$ cells within the fibrous cap (**Fig. 4d**), and within lesions (**Fig. 4f**), but reduced proliferation of SMC-derived cells (**Fig. 4g**) and marked reduction in the YFP$^+$ SMC apoptosis (**Fig. 4h**). These changes were not associated with changes in medial area, lumen area (**Supplementary Fig. 8g**), percent YFP$^+$PDGFβR$^+$ SMC (**Supplementary Fig. 8h**), or YFP$^+$ACTA2$^+$ SMC (**Fig. 4f**). In addition, we did not observe changes in cholesterol, or triglyceride levels (**Supplementary Fig. 8i**).

KLF4 modulates phenotypic transitions and functional properties of SMCs

We have previously presented evidence that *Klf4* is induced in cultured SMCs by treatment with oxidized phospholipids[36] and suppresses expression of SMC marker genes through several mechanisms including binding to the G/C repressor element found in most SMC marker gene promoters including *Acta2, Tagln, and Myh11*, and inhibiting binding of SRF to CARG elements[16, 37, 38]. To determine if similar mechanisms contribute to suppression of SMC marker genes within atherosclerotic lesions *in vivo*, we performed Chromatin Immunoprecipitation (ChIP) assays on chromatin extracted from BCA regions of *Apoe*$^{-/-}$ transgenic mice containing either a wild type *Tagln* promoter driving lacZ or a *Tagln* promoter with a mutation of the GC repressor element (*Tagln* GC repressor mutant lacZ mouse). Results showed marked enrichment of KLF4 binding to *Acta2, Tagln, Myh11*, and *Cnn1* endogenous promoters in Western diet fed animals (**Fig. 5a**). Moreover, we showed that enhanced KLF4 binding to the *Tagln* promoter was dependent on the G/C repressor element (**Fig. 5b**) indicating this repression is mediated through the GC repressor. Finally, we showed that KLF4 is bound to the *Tagln* promoter within individual phenotypically modulated SMC (YFP^{+}ACTA2^{-} cells) within *Apoe*$^{-/-}$ lesions using ISH-PLA (**Fig. 5c**). Taken together, results provide compelling evidence that coordinate suppression of expression of SMC marker genes is mediated by direct binding of KLF4 to the promoters of SMC marker genes.

We[21, 23] and others[39-42] have shown that KLF4 can act as either a transcriptional repressor or activator depending on the cell type and gene locus. To more fully define the repertoire of KLF4 target genes that mediate SMC phenotypic switching, we performed KLF4 ChIP-seq analyses on chromatin samples derived from the BCA from our SMC YFP$^{+/+}$ *Klf4* $^{WT/WT}$ *Apoe*$^{-/-}$ versus SMC YFP$^{+/+}$ *Klf4*$^{\Delta/\Delta}$ *Apoe*$^{-/-}$ mice. This required pooling of BCA samples from 14 mice per group to obtain sufficient DNA. Remarkably, results showed 869 KLF4 target genes (**Fig. 5d**, **Supplementary Table 2**) that were selectively enriched in *Klf4*$^{WT/WT}$ versus *Klf4*$^{\Delta/\Delta}$ *Apoe*$^{-/-}$ Western diet fed mice indicating they represent putative KLF4 target genes selective for SMCs. This included the SMC marker genes *Acta2* and *Tagln*, thus validating the fidelity of our ChIP-Seq analyses. In addition, results provided evidence of enhanced KLF4 enrichment within gene regulatory pathways likely to be important in the pathogenesis of lesions including enrichment of gene families associated with phagocytosis, apoptosis, cell migration, and inflammation (**Fig. 5d, Supplementary Table 2**), which likely contributed to the beneficial overall effects of loss of *Klf4* within SMCs on lesion size and pathogenesis. KLF4 also bound regions near *Itgal* (CD11a), *Itgax* (CD11b), *Itgam* (CD11c) (**Fig. 5d, Supplementary Table 2**), and *Arg1* (data not shown) in *Klf4*$^{WT/WT}$ mice, but not *Klf4*$^{\Delta/\Delta}$ mice. We also noted 459 KLF4 targets in *Klf4*$^{\Delta/\Delta}$ *Apoe*$^{-/-}$ samples that were not present in *Klf4*$^{WT/WT}$ *Apoe*$^{-/-}$ samples (**Supplementary Fig. 9, Supplementary Table 3**).

Given observations that SMC specific loss of *Klf4* was associated with a marked reduction in SMC-derived Mφ-like cells (**Fig. 4f**), we determined if KLF4 is required for transition of cultured SMC to Mφ-like state *in vitro* following cholesterol loading[12]. Due to recent controversies about the origins and purity of SMCs cultured from mouse vessels[43, 44], we utilized our SMC-lineage tracing mice to harvest SMC populations from 8-week old

tamoxifen injected SMC YFP$^{+/+}$ *Apoe*$^{-/-}$ mice. Flow cytometry results showed > 98% YFP^{+} cells (**Supplementary Fig. 10a**), indicating they are derived from mature differentiated SMCs *in vivo* and not a stem cell source as has been speculated[43, 44]. Cholesterol loading of cultured SMCs resulted in increased expression of *Lgals3* (**Fig. 6a**), and increased *Klf4* expression (**Supplementary Fig. 10b**), which were abolished in aortic SMCs derived from SMC YFP$^{+/+}$ *Klf4*$^{\Delta/\Delta}$ mice (**Fig. 6a**). Cholesterol loading was also associated with increased phagocytosis that was KLF4 dependent (**Fig. 6b, c**). Finally, we showed that cholesterol loading resulted in activation of expression of the pro-inflammatory cytokines MCP1, CXCR1, sTNFα, (**Supplementary Fig. 10c-e**), *Lgals3* (**Fig. 6a**), and the MSC markers *Sca1* and *Eng* (**Supplementary Fig. 10f, g**), all through KLF4-dependent mechanisms. In contrast, although cholesterol loading increased *Abca1* expression this was not KLF4-dependent (**Supplementary Fig. 10h**).

Global heterozygous KO of *Klf4* alters plaque pathogenesis

Previous studies using *VE-cadherin*-Cre *Klf4*$^{FL/FL}$ *Apoe*$^{-/-}$ and *LysM*$^{cre/cre}$ *Klf4*$^{FL/FL}$ *Apoe*$^{-/-}$ mouse models provided evidence that KLF4 plays an atheroprotective role in endothelial cells (ECs) and myeloid cells respectively with KO resulting in increased lesion size and changes consistent with enhanced inflammation[41, 42]. Indeed, we have confirmed the latter findings by showing that *LysM*-cre-dependent KO of *Klf4* was associated with increased lesion size (**Supplementary Fig. 11a**) and Sudan IV lipid staining (**Supplementary Fig. 11b**) in *LysM*$^{cre/cre}$ ROSA stop floxed eYFP *Klf4 Apoe*$^{-/-}$ mice. However, unlike previous studies we saw no changes in triglycerides or total cholesterol (**Supplementary Fig. 11c**). We also showed a reduced number of LysM-cre derived LGALS3^{+} cells (**Supplementary Fig. 11d**) based on YFP identification. However, these data are equivocal regarding what cell populations are affected by the loss of *Klf4* in this model since cells other than myeloid cells, including SMC, may activate LysM-cre.

Since loss of *Klf4* in SMCs had the opposite effects, a key unresolved question is whether global conditional loss of *Klf4* in all cell types would be beneficial or detrimental. To test this, we generated tamoxifen-inducible homozygous (ERT-Cre^{+} *Klf4*$^{FL/FL}$*Apoe*$^{-/-}$) and heterozygous *Klf4* (ERT-Cre^{+} *Klf4*$^{FL/WT}$ *Apoe*$^{-/-}$) KO mice, with the latter representing a model of partial inhibition of KLF4 across all cell types thus mimicking potential therapeutic approaches of partial suppression of KLF4. Unfortunately, mice with conditional global homozygous *Klf4* KO had to be euthanized at 8–10 weeks of Western diet feeding due to excessive weight loss, and development of skin lesions, presumably because KLF4 regulates proliferation and differentiation of epithelial cells[45-48]. Tamoxifen treated ERT-Cre^{+} *Klf4*$^{FL/WT}$ *Apoe*$^{-/-}$ mice (ERT-Cre^{+} *Klf4*$^{\Delta/WT}$ *Apoe*$^{-/-}$) demonstrated 50% recombination, the maximum possible recombination for heterozygous KO, in the aorta, liver, and colon (**Supplementary Fig. 12a, b**), but exhibited no changes in body weight, heart weight, or cholesterol and triglyceride levels when compared to ERT-Cre^{-} *Klf4*$^{FL/WT}$ *Apoe*$^{-/-}$ littermate control mice (**Supplementary Fig. 12c**).

Of major interest, ERT-Cre^{+} *Klf4*$^{\Delta/WT}$ *Apoe*$^{-/-}$ mice had similar changes in atherosclerotic lesions as observed in our SMC specific conditional *Klf4* KO mice including a 30% decrease in lesion size (**Supplementary Fig. 13a**), and exhibited several indices of increased plaque

stability, including increased ACTA2 cap coverage (**Supplementary Fig. 13b**), and decreased LGALS3$^+$ lesion area (**Supplementary Fig. 13c**). In addition, they also showed decreased intra-plaque hemorrhage (**Supplementary Fig. 13d**), and decreased apoptosis and proliferation (**Supplementary Fig. 13e, f**). Taken together, these results indicate that loss of one *Klf4* allele globally in all cell types has beneficial overall effects on plaque development, including the ideal therapeutic goal of smaller more stable lesions.

Discussion

Despite numerous papers showing that cultured SMCs down-regulate expression of SMC differentiation marker genes following exposure to environmental cues present in atherosclerotic lesions including cholesterol[12], POVPC[25], PDGFBB[49], and IL-1β[50], the field has relied almost entirely on detection of these markers to ascertain if a given cell within a lesion is a SMC. Indeed, this practice has contributed to the well-established dogma in the field that the role of SMCs within plaques is rather limited, albeit presumed to be beneficial by virtue of phenotypically modulated SMCs secreting extracellular matrix and contributing to fibrous cap formation. Herein we report definitive evidence that > 80% of phenotypically modulated SMCs within BCAs have previously gone undetected and comprise ~30% of the total cellular composition of the lesion. Moreover, we show that phenotypically modulated SMCs transition to multiple phenotypes within lesions including cells that express markers of Mφs, MSCs, and/or MFs. However, of greatest significance, we show that these transitions are functionally important in that selective loss of *Klf4* within SMCs resulted in reduced lesion size, increased fibrous cap thickness, and major reductions in the fraction of SMC-derived Mφ- and MSC-like cells but an increase in ACTA2$^+$ cells within the fibrous cap. In addition, we show that cholesterol loading of cultured SMCs induced KLF4-dependent activation of Mφ and MSC markers; expression of proinflammatory cytokines; and increased phagocytosis. Finally, *in vivo* KLF4 ChIP-seq analyses identified > 800 putative KLF4 regulated genes within SMC including many associated with pro-inflammatory processes. Taken together results provide compelling evidence that transitions in SMC phenotype play a critical role in lesion development, plaque composition, and stability; and for the first time establish that therapeutic targeting aimed at promoting beneficial changes in SMC phenotype may be a viable means of treating advanced atherosclerosis.

A key question is how did loss of *Klf4* within SMCs result in marked reductions in overall lesion size as well as multiple changes consistent with increased plaque stability? Of major significance, we show that these effects were not due to a change in the number of SMC-derived cells within lesions. Recent studies by the Fisher lab[51] found that while some SMCs will express markers of Mφs after cholesterol loading *in vitro*, principal component analyses of microarray data from these cells revealed that they are distinctly different from classical monocytes, Mφs, and dendritic cells; and have reduced phagocytic capacity[51]. Interestingly, we also showed that SMC derived MSC-like lesion cells appeared to be dysfunctional. As such, we postulate that loss of *Klf4* within SMCs resulted in phenotypic transitions that are favorable for plaque pathogenesis including loss of SMC-derived cells with "proinflammatory" Mφ-like properties, and gain of SMC-derived cells that contribute to plaque stabilization through mechanisms and functions yet to be defined. Although it has

long been postulated that SMCs within lesions play a beneficial role (see reviews[9-11, 26, 52, 53]), our studies show this is an over-simplification and can vary dramatically depending on the nature of the SMC phenotypic transitions. A critical challenge for future studies will be to identify the environmental cues within advanced atherosclerotic lesions that regulate phenotypic transitions of SMCs, as well as each of the major cell types within lesions, and to determine how these might be manipulated therapeutically to reduce plaque burden and increase plaque stability.

Online Methods

Mice

Animal protocols were approved by the University of Virginia Animal Care and Use Committee.

Male *Myh11*-CreER^{T2}, *LysM*$^{cre/cre}$, *Apoe*$^{-/-}$, ROSA*26* STOP-flox eYFP$^{+/+}$, *Klf4*$^{FL/FL}$, ERT-Cre, and *Tagln* G/C Repressor mutant mice were used in this study. ROSA*26* STOP-flox eYFP$^{+/+}$ and *Apoe*$^{-/-}$ mice were obtained from Jackson Laboratories. *Myh11*-CreER^{T2}, ROSA26 STOP-flox eYFP, *Klf4*$^{FL/FL}$, and ERT-Cre mice were genotyped by PCR as previously described[56-59]. Cre recombinase was activated in male mice with a series of ten 1 mg tamoxifen intraperitoneal injections (Sigma T-5648) from 6 to 8 weeks of age for a total of 10 mg of tamoxifen per 25 g mouse for both the *Myh11*-CreER^{T2} and ERT-Cre mouse models. *Tagln* G/C Repressor mutant *ApoE*$^{-/-}$ mouse was previously generated and described by our lab[60]. Male littermate controls were utilized for all studies. Next, mice were fed a high-fat diet containing 21% milk fat and 0.15% cholesterol (Harlan Teklad) for 18 weeks starting at the end of tamoxifen treatment. Mice were euthanized by CO_2 asphyxiation and then perfused via the left ventricle as follows: 5 mL PBS, 10 mL 4% paraformaldehyde, 5mL PBS. Brachiocephalic arteries were carefully dissected and fixed for and additional hour in 4% paraformaldehyde before they were embedded in paraffin. Assays for determining total plasma cholesterol and triglyceride levels (Abbott Laboratories) were performed by the University of Virginia Clinical Pathology Laboratory. Mice were allocated to experimental groups based on genotyping and then randomized for the various experimental measurements. Any animal with triglyceride or cholesterol levels outside of three standard deviations were excluded from all future analyses.

Analysis of Atherosclerotic Plaques

Paraffin-embedded brachiocephalic arteries (BCAs) were serially sectioned at 10 μm thickness from the aortic arch to the right subclavian artery. For immunofluorescent analysis of LGALS3^{+} SMCs within the, BCA three sections were taken 300 μm apart, spanning the length of the BCA. Slides were stained with antibodies to GFP (Abcam ab6673), ACTA2 (Sigma F3777), LGALS3 (Cedarlane CL8942AP), MKI67 (Abcam ab15580), CASP3 (Cell Signaling 9661S), KLF4 (R&D Systems AF3158), MYH11 (Kamiya Biomedical Company MC-352), PDGFβR (Abcam ab32570), and SCA1 (Ly6A/E) (Abcam ab51317). Using a Zeiss LSM700 confocal microscope a series of 8 z-stack images of 1 μm thickness were acquired for further analysis. Five 14283 μm^2 locations within each z-stack of every BCA were analyzed using Zen 2009 Light Edition Software for the presence of

immunofluorescent staining coinciding with a single DAPI$^+$ nucleus to determine the average cell populations within each lesion. Every plane of the z-stack was used to assess the co-localization of cellular markers within a single cell. The region of the lesion within 30 μm of the luminal boundary, as determined using Zen 2009 Light Edition Software, was analyzed to determine the cellular composition of the lesion cap, the area within this region was compared to the entire area of the atherosclerotic lesion to determine cap area/lesion area. Morphometric analyses of lesion size were completed using ImagePro Plus as described in Alexander et *al*[61]. Researchers were blinded to the genotype of the animals until the end of the analysis.

Immuno-Transmission Electron Microscopy

18 week WD fed SMC YFP$^{+/+}$ *Apoe*$^{-/-}$ mice were euthanized by CO_2 asphyxiation after 18 weeks of Western diet treatment and perfusion fixed with 0.5% gluteraldehyde (Electron Microscopy Sciences 16300), 4% Paraformaldehyde (Electron Microscopy Sciences 15700) in 1XPBS. Brachiocephalic arteries were isolated, frozen in liquid nitrogen, and sent to the University of Virginia Advanced Microscopy Core for processing. Grids were stained with an antibody to GFP (Abcam ab6673), and followed with a rabbit anti-goat secondary conjugated to 10 nm gold beads (Electron Microscopy Sciences 25229). Images were captured using a JEOL 1230 transmission electron microscope with ultra-high resolution capture camera.

Flow Cytometry

SMC YFP$^{+/+}$ *Apoe*$^{-/-}$ mice were euthanized by CO_2 asphyxiation after 18 weeks of Western diet treatment. Mice were then perfused with 10mL of PBS and the aorta from the iliac bifurcation to the aortic root was gently cleaned of fat and fascia before removal from the animal. Once cleaned, the tissue was placed into an enzyme cocktail containing 4U/mL Liberase TM (Roche 05401119001), 0.1mg/mL DNaseI, and 60U/mL Hyaluronidase in RPMI-1640. Once immersed in the digestion cocktail, the tissue was cut longitudinally, minced, and placed in a 37°C incubator for 1.5 hours. Cells were run through a 70 μm strainer and spun down at 500g for 5 min. Cells were resuspended in red blood cell lysis buffer (BD PharmLyse 555899) for two minutes and then inactivated using serum containing media, spun down again, and resuspended in 200 μL 1XPBS. **Mφ marker** expressing SMCs were identified using antibodies to F4/80 (eBioscience 17-4801), PTPRC (eBioscience 47-0451), ITGAM (eBioscience 45-0112), DAPI (Invitrogen), LGALS3 (BioLegend 125405), and ITGAX (eBioscience 25-0114). **MSCs** were identified using negative gating for PTPRC (eBioscience 12-0451-82), CDH5 (eBioscience 17-1441), and CD34 (BioLegend 128611); and positive gating for ENG (eBioscience 48-1051-82) and SCA1 (eBioscience 45-5981-82). All samples were run on a Beckman Coulter CyAn ADP LX flow cytometer equipped with 405nm, 488nm, and 633nm lasers. Mesenchymal stem cells were isolated using a Becton Dickinson Influx Cell Sorter.

Human Specimens

De-identified coronary arteries specimens from patients (n = 12) collected during autopsy. These specimens were processed, fixed in paraformaldehyde and paraffin-embedded blocks

were cut into 5μm sections. Coronary artery specimen was from a male patient whom received a heart from a female donor (n = 1). The institutional review board at University of Virginia approved the use of all autopsy specimens.

ISH-PLA

ISH-PLA was performed as previously described[57]. Briefly, human *MYH11*, mouse *Myh11*, and mouse *Tagln* probes were generated by Nick Translation (Roche) using biotin-14-dATP (Invitrogen). Biotin labeled probes (40 ng/slide) underwent denaturation in Hybridization Buffer (2× SSC, 50% high grade formamide, 10% dextran sulfate, 1μg of human or mouse Cot-1 DNA) for 5 min at 80°C. After immunostaining for ACTA2 (Sigma F3777), CD68 (Santa Cruz sc20060 KP1 clone), slides were dehydrated in ethanol series and incubated in 1mM EDTA (pH 8.0) for 20 min. Then, samples were incubated with pepsin (0.5%) in buffer (0.05M Tris, 2mM CaCl2, 0.01M EDTA, 0.01M NaCl) at 37°C for 20 min, as previously described[62]. Hybridization mixture containing biotin labeled probes or 5-TAMRA-dUTP labeled Y chromosome probe (Clone RP11-88F4, Empire Genomics) was applied on sections. Sections were incubated at 80°C for 5 min, followed by 16–24h incubation at 37°C. Hybridization was followed by multiple washes in 2× SSC, 0.1% NP-40 buffer. PLA was performed directly after ISH following manufacturer's instructions (Olink) and as previously described (Nature Methods ref) Sections were incubated with mouse H3K4dime (5 μg/mL, clone CMA303 Millipore) and rabbit Biotin (5 μg/mL, # ab53494, Abcam) antibodies overnight at 4°C. The PLA amplification was performed using the Duolink detection kit Orange, 555nm. Finally, mounting medium with DAPI was used to coverslip the slides. Images were acquired with an Olympus BX41 fitted with a Q imaging Retiga 2000R camera. Image acquisition was performed using Q Capture Pro software (Media Cybernetics & QImaging Inc). Settings were fixed at the beginning of both acquisition and analysis steps and were unchanged. Brightness and contrast were equally adjusted after merging. Image analysis was performed with Image J. To estimate the percentage of SMC-derived Mφ-like cells, the number of $CD68^+/PLA^+$ cells in CD68 positive staining areas of human coronary lesions (n = 12). We previously rigorously estimated the efficiency of the ISH-PLA method in mouse and human tissues that reaches 65%[57]. Thus, the percentage of the $CD68^+/PLA^+$ cells counted in human lesions is corrected considering the incomplete efficiency of ISH-PLA.

ChIP Assays

Cell culture ChIP was performed as previously described[63]. Cells were fixed with 1% paraformaldehyde for 10 min at room temperature. The cross-linked chromatin was sonicated to shear chromatin into fragments of 200–600 base pairs. The sheared chromatin was immunoprecipitated with 2 μg of dimeH3K4 (clone CMA303, Millipore), or KLF4 (Santa Cruz sc20691) while negative control was incubated with mouse or rabbit IgG. Immune complexes were captured with magnetic bead-coupled protein G (Millipore). After elution and purification of the genomic DNA (gDNA), real time PCR was performed on IP and non-immunoprecipitated INPUT gDNA. Primer sets used for *Myh11*, *Arg1* and *Cox2* promoters were previously described[57, 64]. Results are expressed as the percentage of IP/INPUT. *In vivo* KLF4 ChIP assays were performed using flash frozen BCAs from mice that

had been fed either 18 weeks of high-fat or standard chow (Harlan 7012) beginning at 8 weeks of age as previously described[65, 66].

KLF4 Chromatin Immunoprecipitation Sequencing (ChIP-seq)

Segments of the aorta from the arch to the aortic root and up to the carotid bifurcations were isolated from 18 week WD fed SMC *Klf4*$^{WT/WT}$ eYFP$^{+/+}$ *Apoe*$^{-/-}$ (n = 14), SMC *Klf4*$^{\Delta/\Delta}$ eYFP$^{+/+}$ *Apoe*$^{-/-}$ (n = 14), and 8 week old chow fed SMC *Klf4*$^{WT/WT}$ eYFP$^{+/+}$ *Apoe*$^{-/-}$ (n = 15) were snap frozen in liquid nitrogen and then processed as mentioned in ChIP methods section for KLF4 binding. DNA library preparation and deep sequencing was performed by HudsonAlpha Institute for Biotechnology via Illumina TruSeq Chip Library Kit according to the manufacturer's protocol. Quality control and quantification of DNA and library were performed using Agilent 2100 Bioanalyser and Kapa Library Quant Kit according to manufacturer's protocol.

ChIP-seq data processing

The sequencing reads from Illumina HiSeq were aligned to the mouse genome (mm10) using the BOWTIE alignment tool[67]. These aligned reads were then processed and converted into bam/bai (http://genome.ucsc.edu/goldenPath/help/bam.html) format, and then loaded in the Integrative Genomics Viewer (http://www.broadinstitute.org/igv/) for visualization. The processing steps involved removing duplicate reads and format conversions using SAMtools[68] suite. The reads were also converted to BED format (http://genome.ucsc.edu/FAQ/FAQformat#format1) for further data analysis processes such as peak calling. Peak finding was performed using MACS14 (ref. 69) with ChIP-seq BED files as input, default parameters ($P = 1 \times 10^{-5}$). Once the peaks were obtained for all the tracks, the common peaks and genes between these tracks were removed by BEDtools[70] intersect command. The outcome of the above filtering steps resulted in signals present, theoretically, in KLF4 bound to genes within SMC. Functional annotation was performed using PANTHER[71] and Gene Ontology Consortium (http://geneontology.org/) and statistical over representation test was performed using PANTHER[71]. GEO accession number GSE65812.

Cell Culture Studies

Primary mouse aortic SMCs were isolated from 8 week old SMC-lineage tracing mice after a series of 10 tamoxifen injections using a previously described protocol[72]. Cells isolated from SMC YFP$^{+/+}$ *Klf4*$^{WT/WT}$ and SMC YFP$^{+/+}$ *Klf4*$^{\Delta/\Delta}$ mice were passaged three times before undergoing a cell selective sort for YFP+. Cholesterol assays were performed using water-soluble cholesterol from Sigma (C4951-30MG) as previously published[73] with minor modification: Cholesterol was reconstituted in DMEM-F12 media from Gibco containing; 0.2% FBS (Gibco); 100 U/mL penicillin/streptomycin (Gibco); 1.6 mmol/l L-glutamine, (Gibco). Cells were allowed to grow to ~70% confluency before being switched to 0, 20, 40, or 80 μg/mL cholesterol containing media. After 72hrs cells were harvested for mRNA, protein, or ChIP analysis. Human coronary SMC were purchased from Lonza and cultured in SMC maintaining media (Lonza). RAW264.7 mouse Mφs and human monocytes were cultured as previously described.

Bead Uptake Assays

Primary mouse aortic SMCs were treated with cholesterol as aforementioned. After 72hrs cells were switched back to DF10 media containing 1.5% v/v 0.84μm polysterene beads (Spherotech FP-0870-2) for 1.5 hours. Cells were then harvested, stained with LGALS3 (BioLegend 125405) and run on an Amnis ImageStreamX Mark II using a 60X objective. Data was analyzed using Amnis IDEAS software.

Mesenchymal Stem Cell Differentiation

Cells were isolated from 12, 18 week Western diet fed SMC $YFP^{+/+}$ *Apoe*$^{-/-}$ mice as described in the flow cytometry section. Next, cells were stained with markers for lin^- ($CD34^-$ BioLegend 128611, $PTPRC^-$ eBioscience 56-0451-80, CDH5 – eBioscience 17-1441-80); and positive gating for ENG (eBioscience 48-1051-82) and SCA1 (eBioscience 45-5981-82). YFP was detected by native fluorescence. Cells were then sorted into four populations ($YFP^+SCA1^+ENG^+$, $YFP^-SCA1^+ENG^+$, $YFP^+SCA1^-ENG^-$, and $YFP^-SCA1^-ENG^-$) using a Becton Dickinson Influx Cell Sorter. Cells were then placed at in StemXVivo MSC media (R&D Systems CCM004) media at a density of 30,000 cells/mm^2 and were passed at 70% confluency (changing media every 2–3 days). YFP^+, $SCA1^+$, ENG^+ cells were p2 for differentiation experiment, and YFP^-, $SCA1^+$, ENG^+ cells were p4 at the start of the differentiation experiment. Differentiation experiment was conducted using a kit from R&D systems (mouse mesenchymal stem cell functional differentiation kit, SC010). Cells were differentiated in the appropriate media for 14 days (changing media every 2–3 days), then fixed and immunocytochemistry utilizing antibodies from the kit and performed according to the protocol provided.

Statistics

Fisher's exact test was used for categorical data. Two-way ANOVA with Tukey post-hoc tests were used for multiple group comparisons determined to have normal distribution by the Kolmogorov-Smirnov test. Two analyses showed statistical difference across multiple locations, ACTA2/DAPI, and YFP/DAPI, using 2-way ANOVA. All other analyses across multiple locations were therefore not reported in the manuscript. Non-parametric data were analyzed using the Wilcoxon rank sum test. There were no significant interactions between genotype and location for any of the end points analyzed by the 2-way ANOVA. $P < 0.05$ was considered significant. SAS v9.3 with Enterprise Guide v5.1 software (SAS Institute Inc.) was used for all statistical analyses.

Supplementary Material

Refer to Web version on PubMed Central for supplementary material.

Acknowledgements

We would like to acknowledge the valuable contributions of technicians M. McCanna and M.Bevard for their assistance in histological cutting and staining, R. Tripathi for assistance with cell culture work; J. Lannigan and M. Solga from the Flow Cytometry Core at UVA for their help designing flow cytometry panels and help running the cytometers; S. Guilot at the Advanced Microscopy Facility at UVA for her help running the TEM, J. Roithmayr, N. Hendley, M. Quetsch and M. Goodwin for their assistance in immunofluorescent image analysis; Y. Babiy for designing the cartoon in Supplementary Fig. 6, and W. Evans for assistance in processing statistical analyses. We

would also like to thank N. McGinn from the Department of Pathology, University of Virginia Hospital for the de-identified coronary arteries specimens, C. Murray from the University of Washington for the coronary artery heart transplant specimen, S. Offermanns from the Max Planck Institute[54] for the *Myh11*-CreER^{T2} mice, Kaestner for the *Klf4*$^{FL/FL}$ (ref. 47) mice, G. Randolph for the *LysM*$^{cre/cre}$ mice, and A. Berns from the Netherlands Cancer Institute, Amsterdam, Netherlands for the transgenic tamoxifen-inducible Cre (ERT-Cre) recombinase mice[55]. This work was supported by US National Institutes of Health R01 grants HL057353, HL098538, and HL087867 to G.K.O., HL112904 to ACS, as well as a pilot grant from AstraZeneca Pharmaceutical as part of a University of Virginia – AstraZeneca Research Alliance; and Mid-Atlantic American Heart Association fellowship grants 11PRE7170008, and 13POST17080043 to L.S.S., and D.G. respectively.

Reference List

1. Saffitz JE, Schwartz CJ. Coronary atherosclerosis and thrombosis underlying acute myocardial infarction. Cardiol. Clin. 1987; 5:21–30. [PubMed: 3548973]
2. Libby P, Aikawa M. Stabilization of atherosclerotic plaques: new mechanisms and clinical targets. Nat. Med. 2002; 8:1257–1262. [PubMed: 12411953]
3. Falk E, Nakano M, Benton JF, Finn AV, Virmani R. Update on acute coronary syndromes: the pathologists' view. Eur. Heart J. 2012
4. Falk E, Shah PK, Fuster V. Coronary plaque disruption. Circulation. 1995; 92:657–671. [PubMed: 7634481]
5. Virmani R, Kolodgie FD, Burke AP, Farb A, Schwartz SM. Lessons from sudden coronary death: a comprehensive morphological classification scheme for atherosclerotic lesions. Arterioscler. Thromb. Vasc. Biol. 2000; 20:1262–1275. [PubMed: 10807742]
6. Lee RT, Libby P. The unstable atheroma. Arterioscler. Thromb. Vasc. Biol. 1997; 17:1859–1867. [PubMed: 9351346]
7. Ross R. Atherosclerosis--an inflammatory disease. N. Engl. J. Med. 1999; 340:115–126. [PubMed: 9887164]
8. Libby P. Inflammation in atherosclerosis. Arterioscler. Thromb. Vasc. Biol. 2012; 32:2045–2051. [PubMed: 22895665]
9. Glass CK, Witztum JL. Atherosclerosis. the road ahead. Cell. 2001; 104:503–516. [PubMed: 11239408]
10. Libby P, Ridker PM, Hansson GK. Progress and challenges in translating the biology of atherosclerosis. Nature. 2011; 473:317–325. [PubMed: 21593864]
11. Gomez D, Owens GK. Smooth muscle cell phenotypic switching in atherosclerosis. Cardiovasc. Res. 2012; 95:156–164. [PubMed: 22406749]
12. Rong JX, Shapiro M, Trogan E, Fisher EA. Transdifferentiation of mouse aortic smooth muscle cells to a macrophage-like state after cholesterol loading. Proc. Natl. Acad. Sci. U. S. A. 2003; 100:13531–13536. [PubMed: 14581613]
13. Martin K, et al. Thrombin stimulates smooth muscle cell differentiation from peripheral blood mononuclear cells via protease-activated receptor-1, RhoA, and myocardin. Circ. Res. 2009; 105:214–218. [PubMed: 19574550]
14. Caplice NM, et al. Smooth muscle cells in human coronary atherosclerosis can originate from cells administered at marrow transplantation. Proc. Natl. Acad. Sci. U. S. A. 2003; 100:4754–4759. [PubMed: 12665618]
15. Iwata H, et al. Bone marrow-derived cells contribute to vascular inflammation but do not differentiate into smooth muscle cell lineages. Circulation. 2010; 122:2048–2057. [PubMed: 21041690]
16. Wamhoff BR, et al. A G/C element mediates repression of the SM22alpha promoter within phenotypically modulated smooth muscle cells in experimental atherosclerosis. Circ. Res. 2004; 95:981–988. [PubMed: 15486317]
17. Feil S, et al. Transdifferentiation of vascular smooth muscle cells to macrophage-like cells during atherogenesis. Circ. Res. 2014; 115:662–667. [PubMed: 25070003]
18. Swirski FK, Nahrendorf M. Do vascular smooth muscle cells differentiate to macrophages in atherosclerotic lesions? Circ. Res. 2014; 115:605–606. [PubMed: 25214571]

19. Allahverdian S, Chehroudi AC, McManus BM, Abraham T, Francis GA. Contribution of Intimal Smooth Muscle Cells to Cholesterol Accumulation and Macrophage-Like Cells in Human Atherosclerosis. 2014
20. Cordes KR, et al. miR-145 and miR-143 regulate smooth muscle cell fate and plasticity. Nature. 2009; 460:705–710. [PubMed: 19578358]
21. Yoshida T, Kaestner KH, Owens GK. Conditional deletion of Kruppel-like factor 4 delays downregulation of smooth muscle cell differentiation markers but accelerates neointimal formation following vascular injury. Circ. Res. 2008; 102:1548–1557. [PubMed: 18483411]
22. Deaton RA, Gan Q, Owens GK. Sp1-dependent activation of KLF4 is required for PDGF-BB-induced phenotypic modulation of smooth muscle. Am. J. Physiol Heart Circ. Physiol. 2009; 296:H1027–H1037. [PubMed: 19168719]
23. Yoshida T, Gan Q, Owens GK. Kruppel-like factor 4, Elk-1, and histone deacetylases cooperatively suppress smooth muscle cell differentiation markers in response to oxidized phospholipids. Am. J. Physiol Cell Physiol. 2008; 295:C1175–C1182. [PubMed: 18768922]
24. Thomas JA, et al. PDGF-DD, a novel mediator of smooth muscle cell phenotypic modulation, is upregulated in endothelial cells exposed to atherosclerosis-prone flow patterns. Am. J. Physiol Heart Circ. Physiol. 2009; 296:H442–H452. [PubMed: 19028801]
25. Pidkovka NA, et al. Oxidized phospholipids induce phenotypic switching of vascular smooth muscle cells in vivo and in vitro. Circ. Res. 2007; 101:792–801. [PubMed: 17704209]
26. Alexander MR, Owens GK. Epigenetic Control of Smooth Muscle Cell Differentiation and Phenotypic Switchingin Vascular Development and Disease. Annu. Rev. Physiol. 2011
27. Gomez D, Shankman LS, Nguyen AT, Owens GK. Detection of histone modifications at specific gene loci in single cells in histological sections. Nat. Methods. 2013; 10:171–177. [PubMed: 23314172]
28. Klein D, Benchellal M, Kleff V, Jakob HG, Ergun S. Hox genes are involved in vascular wall-resident multipotent stem cell differentiation into smooth muscle cells. Sci. Rep. 2013; 3:2178. [PubMed: 24145756]
29. Klein D, et al. Vascular wall-resident CD44+ multipotent stem cells give rise to pericytes and smooth muscle cells and contribute to new vessel maturation. PLoS. One. 2011; 6:e20540. [PubMed: 21637782]
30. Xiao Q, et al. Sca-1+ progenitors derived from embryonic stem cells differentiate into endothelial cells capable of vascular repair after arterial injury. Arterioscler. Thromb. Vasc. Biol. 2006; 26:2244–2251. [PubMed: 16902164]
31. Xiao Q, Zeng L, Zhang Z, Hu Y, Xu Q. Stem cell-derived Sca-1+ progenitors differentiate into smooth muscle cells, which is mediated by collagen IV-integrin alpha1/beta1/alphav and PDGF receptor pathways. Am. J. Physiol Cell Physiol. 2007; 292:C342–C352. [PubMed: 16914533]
32. Passman JN, et al. A sonic hedgehog signaling domain in the arterial adventitia supports resident Sca1+ smooth muscle progenitor cells. Proc. Natl. Acad. Sci. U. S. A. 2008; 105:9349–9354. [PubMed: 18591670]
33. McDonald OG, Wamhoff BR, Hoofnagle MH, Owens GK. Control of SRF binding to CArG box chromatin regulates smooth muscle gene expression in vivo. J. Clin. Invest. 2006; 116:36–48. [PubMed: 16395403]
34. Vladykovskaya E, et al. Reductive metabolism increases the proinflammatory activity of aldehyde phospholipids. J. Lipid Res. 2011; 52:2209–2225. [PubMed: 21957201]
35. Takahashi K, et al. Induction of pluripotent stem cells from adult human fibroblasts by defined factors. Cell. 2007; 131:861–872. [PubMed: 18035408]
36. Cherepanova OA, et al. Oxidized phospholipids induce type VIII collagen expression and vascular smooth muscle cell migration. Circ. Res. 2009; 104:609–618. [PubMed: 19168440]
37. Salmon M, Gomez D, Greene E, Shankman L, Owens GK. Cooperative binding of KLF4, pELK-1, and HDAC2 to a G/C repressor element in the SM22alpha promoter mediates transcriptional silencing during SMC phenotypic switching in vivo. Circ. Res. 2012; 111:685–696. [PubMed: 22811558]

38. Regan CP, Adam PJ, Madsen CS, Owens GK. Molecular mechanisms of decreased smooth muscle differentiation marker expression after vascular injury. J. Clin. Invest. 2000; 106:1139–1147. [PubMed: 11067866]
39. Feinberg MW, et al. The Kruppel-like factor KLF4 is a critical regulator of monocyte differentiation. EMBO J. 2007; 26:4138–4148. [PubMed: 17762869]
40. Liao X, et al. Kruppel-like factor 4 regulates macrophage polarization. J. Clin. Invest. 2011; 121:2736–2749. [PubMed: 21670502]
41. Sharma N, et al. Myeloid Kruppel-like factor 4 deficiency augments atherogenesis in ApoE−/− mice--brief report. Arterioscler. Thromb. Vasc. Biol. 2012; 32:2836–2838. [PubMed: 23065827]
42. Zhou G, et al. Endothelial Kruppel-like factor 4 protects against atherothrombosis in mice. J. Clin. Invest. 2012; 122:4727–4731. [PubMed: 23160196]
43. Nguyen AT, et al. Smooth muscle cell plasticity: fact or fiction? Circ. Res. 2013; 112:17–22. [PubMed: 23093573]
44. Tang Z, et al. Differentiation of multipotent vascular stem cells contributes to vascular diseases. Nat. Commun. 2012; 3:875. [PubMed: 22673902]
45. Foster KW, et al. Induction of KLF4 in basal keratinocytes blocks the proliferation-differentiation switch and initiates squamous epithelial dysplasia. Oncogene. 2005; 24:1491–1500. [PubMed: 15674344]
46. Jaubert J, Cheng J, Segre JA. Ectopic expression of kruppel like factor 4 (Klf4) accelerates formation of the epidermal permeability barrier. Development. 2003; 130:2767–2777. [PubMed: 12736219]
47. Katz JP, et al. The zinc-finger transcription factor Klf4 is required for terminal differentiation of goblet cells in the colon. Development. 2002; 129:2619–2628. [PubMed: 12015290]
48. Katz JP, et al. Loss of Klf4 in mice causes altered proliferation and differentiation and precancerous changes in the adult stomach. Gastroenterology. 2005; 128:935–945. [PubMed: 15825076]
49. Dandre F, Owens GK. Platelet-derived growth factor-BB and Ets-1 transcription factor negatively regulate transcription of multiple smooth muscle cell differentiation marker genes. Am. J. Physiol Heart Circ. Physiol. 2004; 286:H2042–H2051. [PubMed: 14751865]
50. Clement N, et al. Notch3 and IL-1beta exert opposing effects on a vascular smooth muscle cell inflammatory pathway in which NF-kappaB drives crosstalk. J. Cell Sci. 2007; 120:3352–3361. [PubMed: 17881497]
51. Vengrenyuk Y, et al. Cholesterol Loading Reprograms the MicroRNA-143/145-Myocardin Axis to Convert Aortic Smooth Muscle Cells to a Dysfunctional Macrophage-Like Phenotype. Arterioscler Thromb Vasc Biol. 2015; 35:535–546. [PubMed: 25573853]
52. Owens GK. Regulation of differentiation of vascular smooth muscle cells. Physiol Rev. 1995; 75:487–517. [PubMed: 7624392]
53. Owens GK, Kumar MS, Wamhoff BR. Molecular regulation of vascular smooth muscle cell differentiation in development and disease. Physiol Rev. 2004; 84:767–801. [PubMed: 15269336]
54. Wirth A, et al. G12-G13-LARG-mediated signaling in vascular smooth muscle is required for salt-induced hypertension. Nat. Med. 2008; 14:64–68. [PubMed: 18084302]
55. Vooijs M, Jonkers J, Berns A. A highly efficient ligand-regulated Cre recombinase mouse line shows that LoxP recombination is position dependent. EMBO Rep. 2001; 2:292–297. [PubMed: 11306549]
56. Wirth A, et al. G12-G13-LARG-mediated signaling in vascular smooth muscle is required for salt-induced hypertension. Nat. Med. 2008; 14:64–68. [PubMed: 18084302]
57. Gomez D, Shankman LS, Nguyen AT, Owens GK. Detection of histone modifications at specific gene loci in single cells in histological sections. Nat. Methods. 2013; 10:171–177. [PubMed: 23314172]
58. Katz JP, et al. The zinc-finger transcription factor Klf4 is required for terminal differentiation of goblet cells in the colon. Development. 2002; 129:2619–2628. [PubMed: 12015290]
59. Vooijs M, Jonkers J, Berns A. A highly efficient ligand-regulated Cre recombinase mouse line shows that LoxP recombination is position dependent. EMBO Rep. 2001; 2:292–297. [PubMed: 11306549]

60. Wamhoff BR, et al. A G/C element mediates repression of the SM22alpha promoter within phenotypically modulated smooth muscle cells in experimental atherosclerosis. Circ. Res. 2004; 95:981–988. [PubMed: 15486317]

61. Alexander MR, et al. Genetic inactivation of IL-1 signaling enhances atherosclerotic plaque instability and reduces outward vessel remodeling in advanced atherosclerosis in mice. J. Clin. Invest. 2012; 122:70–79. [PubMed: 22201681]

62. Caplice NM, et al. Smooth muscle cells in human coronary atherosclerosis can originate from cells administered at marrow transplantation. Proc. Natl. Acad. Sci. U. S. A. 2003; 100:4754–4759. [PubMed: 12665618]

63. McDonald OG, Owens GK. Programming smooth muscle plasticity with chromatin dynamics. Circ. Res. 2007; 100:1428–1441. [PubMed: 17525382]

64. Liao X, et al. Kruppel-like factor 4 regulates macrophage polarization. J. Clin. Invest. 2011; 121:2736–2749. [PubMed: 21670502]

65. Deaton RA, Gan Q, Owens GK. Sp1-dependent activation of KLF4 is required for PDGF-BB-induced phenotypic modulation of smooth muscle. Am. J. Physiol Heart Circ. Physiol. 2009; 296:H1027–H1037. [PubMed: 19168719]

66. Salmon M, Gomez D, Greene E, Shankman L, Owens GK. Cooperative binding of KLF4, pELK-1, and HDAC2 to a G/C repressor element in the SM22alpha promoter mediates transcriptional silencing during SMC phenotypic switching in vivo. Circ. Res. 2012; 111:685–696. [PubMed: 22811558]

67. Langmead B, Trapnell C, Pop M, Salzberg SL. Ultrafast and memory-efficient alignment of short DNA sequences to the human genome. Genome Biol. 2009; 10:R25. [PubMed: 19261174]

68. Li H, et al. The Sequence Alignment/Map format and SAMtools. Bioinformatics. 2009; 25:2078–2079. [PubMed: 19505943]

69. Zhang Y, et al. Model-based analysis of ChIP-Seq (MACS). Genome Biol. 2008; 9:R137. [PubMed: 18798982]

70. Quinlan AR, Hall IM. BEDTools: a flexible suite of utilities for comparing genomic features. Bioinformatics. 2010; 26:841–842. [PubMed: 20110278]

71. Mi H, Muruganujan A, Casagrande JT, Thomas PD. Large-scale gene function analysis with the PANTHER classification system. Nat. Protoc. 2013; 8:1551–1566. [PubMed: 23868073]

72. Geisterfer AA, Peach MJ, Owens GK. Angiotensin II induces hypertrophy, not hyperplasia, of cultured rat aortic smooth muscle cells. Circ. Res. 1988; 62:749–756. [PubMed: 3280155]

73. Rong JX, Shapiro M, Trogan E, Fisher EA. Transdifferentiation of mouse aortic smooth muscle cells to a macrophage-like state after cholesterol loading. Proc. Natl. Acad. Sci. U. S. A. 2003; 100:13531–13536. [PubMed: 14581613]

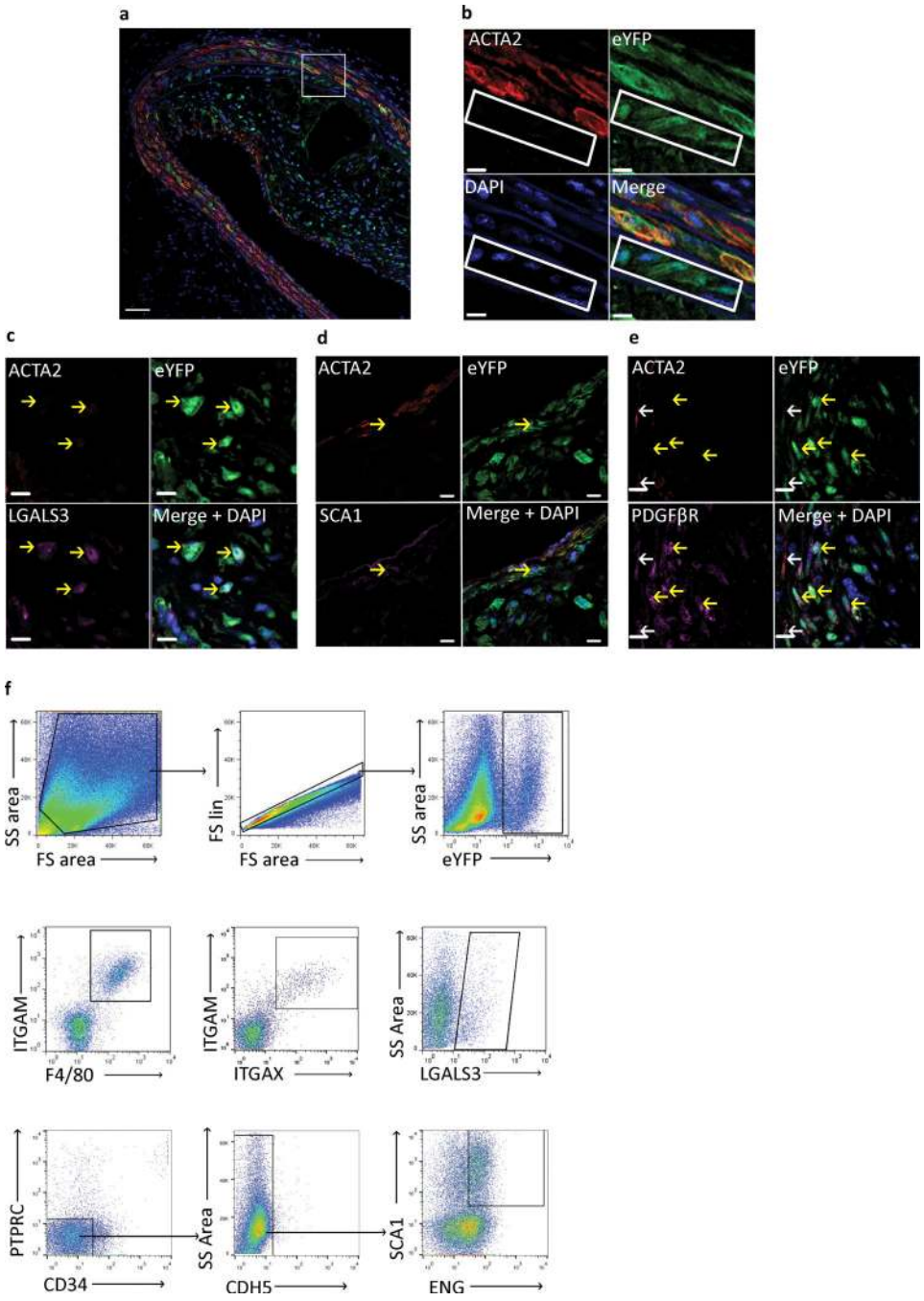

Figure 1. SMC lineage tracing provides evidence for large populations of phenotypically modulated SMCs within BCAs of 18 Week WD fed SMC eYFP$^{+/+}$ *Apoe*$^{-/-}$ mice

Immunofluorescence staining of representative BCAs from 18 week Western diet fed SMC eYFP$^{+/+}$ *Apoe*$^{-/-}$ mice. Results show that differentiated SMCs present at the time of tamoxifen injection (YFP^{+}) subsequently give rise to multiple phenotypes including: (**a**, **b**) phenotypically modulated SMCs (YFP^{+}ACTA2^{-} cells highlighted in white rectangle), (**c**) Mφ-like SMCs (YFP^{+}ACTA2^{-}LGALS3^{+}), (**d**) mesenchymal stem cell-like SMCs (YFP^{+}ACTA2^{-}SCA1^{+}), and (**e**) MF-like cells (YFP^{+}ACTA2^{+}PDGFβR^{+}). Scale bar

represents 50μm (**a**) and 10μm (**b**-**e**). (**c**-**e**) Yellow arrows indicate de-differentiated (YFP^+/$ACTA2^-$) SMCs, white arrows indicate differentiated (YFP^+/$ACTA2^+$) SMCs. Samples were either fixed and embedded in paraffin (**a**-**c**, **e**) or Neg40 (**d**). (**f**) Flow cytometry of single cell suspension from 18 Week WD fed SMC $eYFP^{+/+}$ $Apoe^{-/-}$ mouse aortas to further assess phenotypically modulated SMC populations. The gating strategy included: forward versus side scatter gate; a singlets gate; and YFP+ cell gate. Sub-populations of YFP+ cells were found to be double positive for ITGAM (CD11b) and F4/80, ITGAM (CD11b) and ITGAX (CD11c), LGALS3 (mac2), and double positive for SCA1 and ENG after going through lin^- gating, $n = 6$ animals.

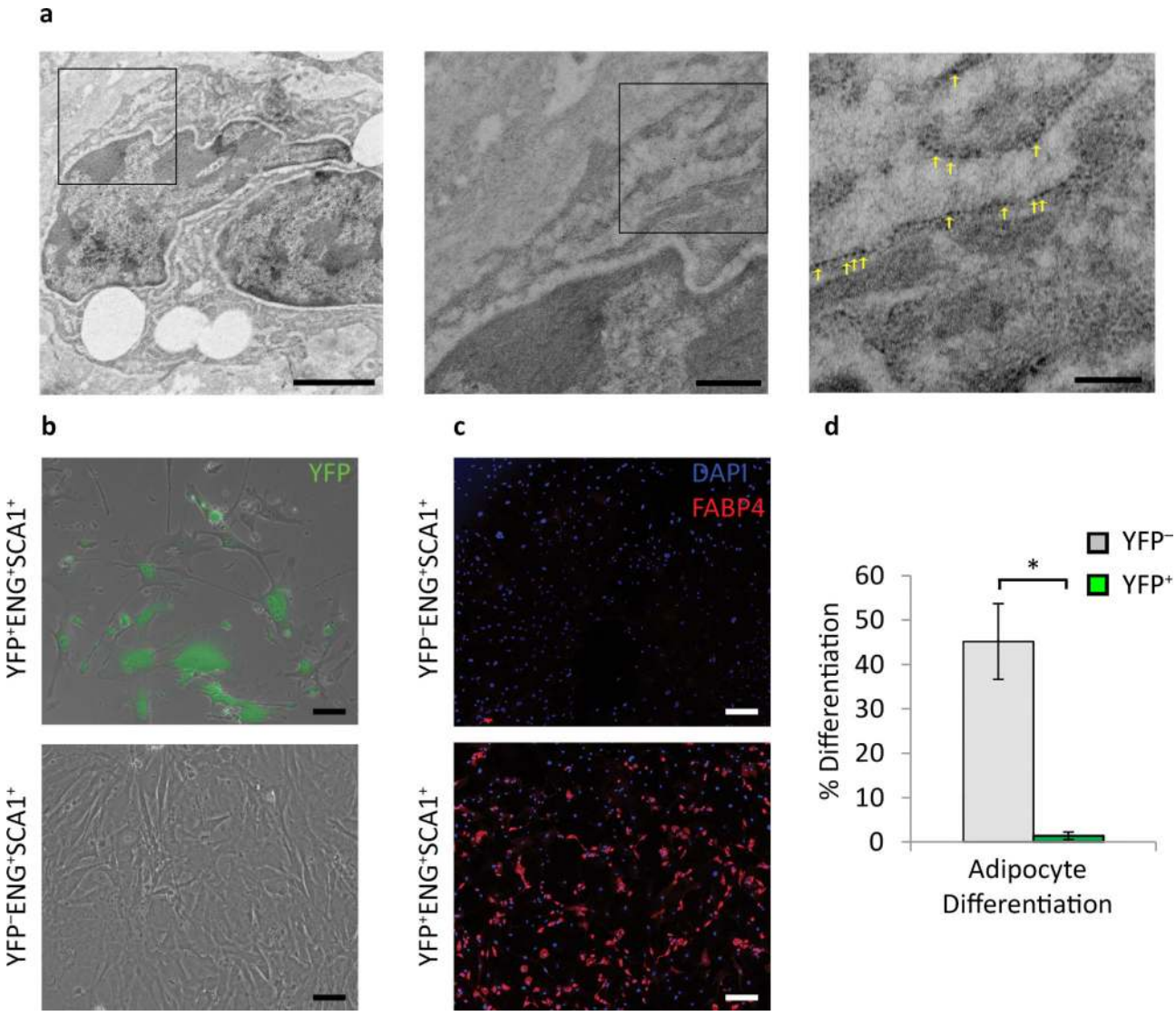

Figure 2. Phenotypically modulated Mφ-like SMCs take on some functional characteristics of Mφs, but MSC-like SMCs show impaired growth and are not multi-potential

(**a**) Immuno-TEM of BCAs from 18 week Western diet SMC eYFP$^{+/+}$ *Apoe*$^{-/-}$ mice using a 10 nm gold bead conjugated secondary antibody revealed lipid laden YFP^{+} cells engulfing neighboring cells. Yellow arrows indicate immuno-gold beads. Scale bars (from left to right): 2 μm, 0.5 μm, 0.2 μm. (**b**) Isolated YFP^{+} and YFP^{-} MSCs (SCA1^{+}ENG^{+}) in mesenchymal stem cell media 10 days post plating, green is native YFP signal. (**c**) YFP^{+} and YFP^{-} MSCs (SCA1^{+}ENG^{+}) after adipogeneisis differentiation based on adipocyte marker FABP4 staining. Scale bar = 200 μm. (**d**) quantification of adipogenesis from five fields of view per group. Error bars = S.D. * $P < 0.05$ by Student's *t*-test.

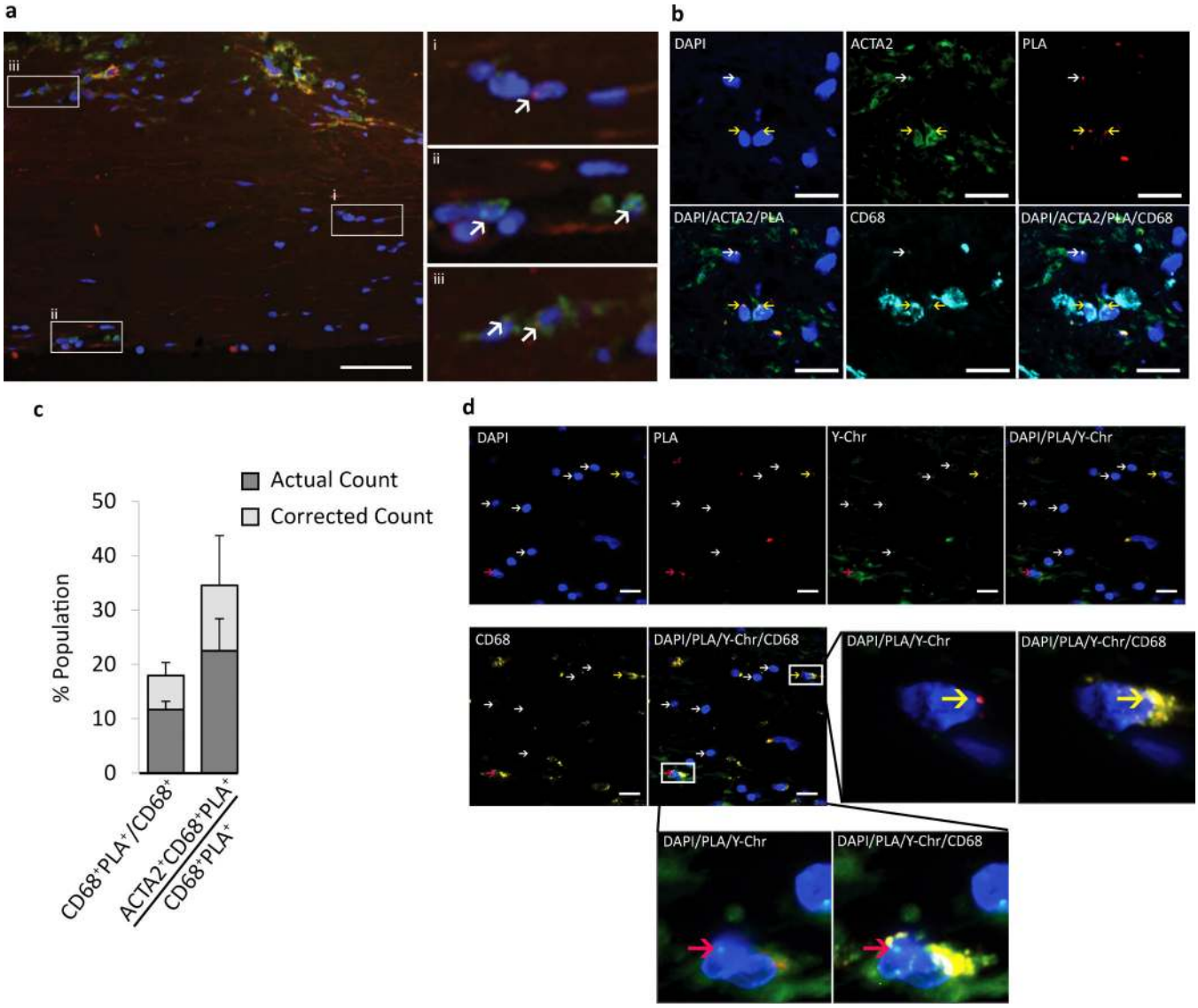

Figure 3. SMCs within human coronary artery lesions express the Mφ marker CD68

(**a**) SMCs within advanced atherosclerotic lesion specimens were identified based on PLA detection of the SMC specific stable epigenetic signature H3K4dime on the *MYH11*[27]. *MYH11* H3K4dime PLA$^+$ cells exhibit a punctate red dot within the nucleus while the non-nuclear amorphous red staining is autofluorescence or non-specific background. (**a**) Samples were also immuno-stained for CD68 (green), and DAPI (blue). Results showed three distinct cell populations highlighted in enlarged panels to the right and indicated with white arrows: (i) *MYH11* H3K4dime PLA$^+$ SMCs that are CD68$^-$, (ii) *MYH11* H3K4dime PLA$^-$CD68$^+$ (HSC-derived Mφs), and (iii) H3K4dime *MYH11* H3K4dime PLA$^+$CD68$^+$ SMC-derived Mφ-like cells. Scale bar = 100 μm. (**b**) Shoulder regions within plaques [stained with DAPI (blue), ACTA2 (green), PLA (red), and CD68 (cyan)] exhibited a high incidence of SMC-derived Mφ-like cells (*MYH11* H3K4dime PLA$^+$CD68$^+$) (yellow arrows) and several phenotypically modulated SMCs negative for CD68 (*MYH11* H3K4dime PLA$^+$ACTA2$^-$ CD68$^-$) (white arrows). Scale bar = 50 μm. (**c**) Quantitative analysis of SMC-derived Mφ-

like cells within human coronary lesions based on *MYH11* H3K4dime ISH-PLA +/− adjustment for the efficiency of PLA[27]. Error bars = S.E.M. for 12 independent samples of human atherosclerosis in the right coronary artery. (**d**) Combined epigenetic SMC and genetic HSC lineage tracing analyses of cross gender human heart transplant samples. Coronary artery specimens from a male patient who received a female heart were processed for *MYH11* H3K4dime PLA (red), Y-chromosome FISH (green), and CD68 staining (yellow). Results show cells that were *MYH11* H3K4dime PLA^+ Y-$chromosome^-$ and $CD68^+$ (yellow arrows) reflecting a SMC-derived Mφ-like cell not of hematopoietic origin (top). In contrast, Mφs of hematopoietic origin are *MYH11* H3K4dime PLA^-Y-$chromosome^+CD68^+$ (red arrows) (bottom). Scale bar = 50 μm.

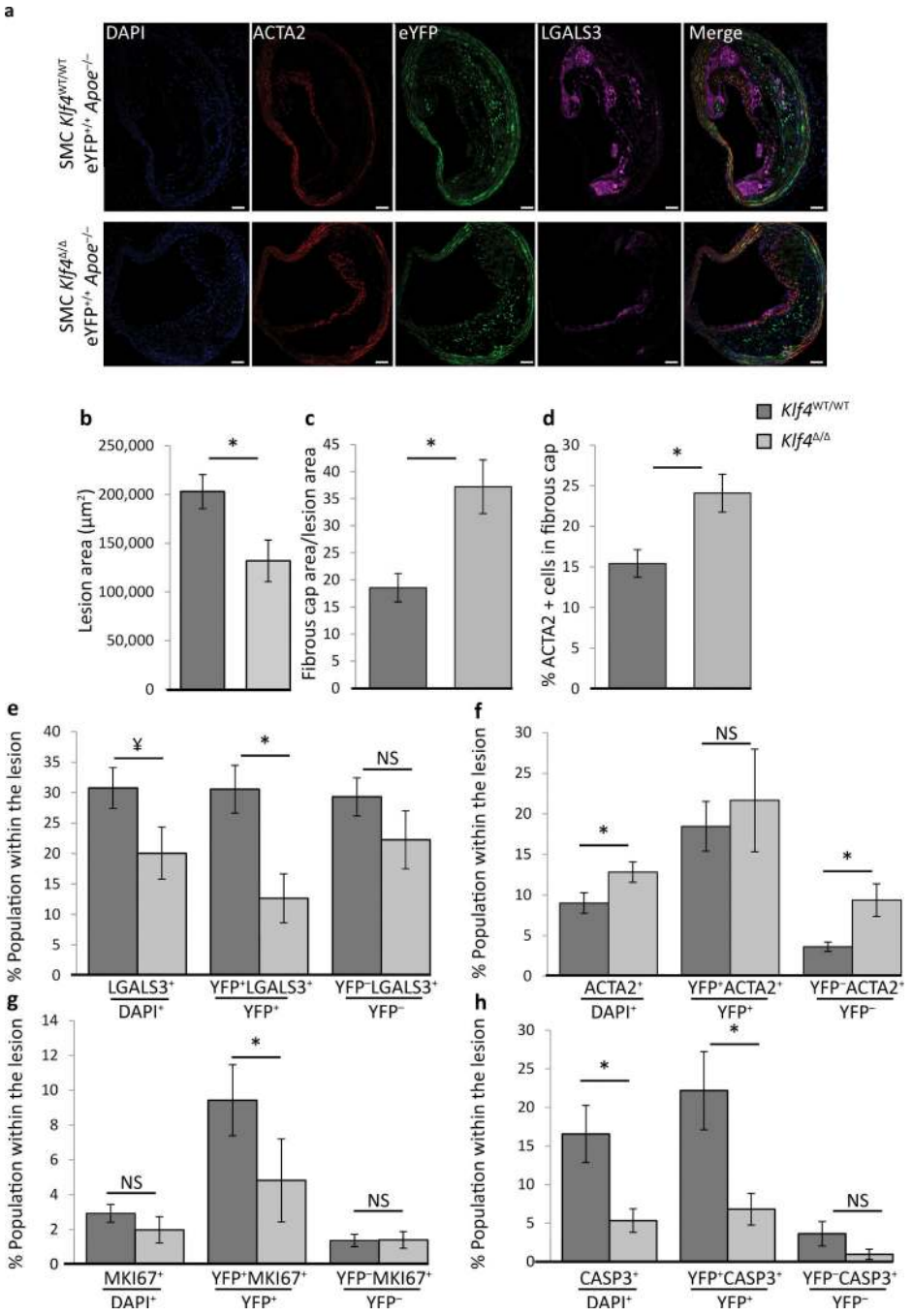

Figure 4. SMC specific *Klf4* conditional KO in *Apoe*$^{-/-}$ mice fed a high fat diet for 18 weeks resulted in decreased lesion size and increased indices of plaque stability

SMC eYFP$^{+/+}$ *Apoe*$^{-/-}$ mice crossed to *Klf4*$^{FL/FL}$ mice were tamoxifen treated and given Western diet for 18 weeks prior to analysis. (**a**) Representative image demonstrating the changes in lesion morphology and cell composition. Results showed the following: (**b**) decreased total lesion area, (**c**) increased fibrous cap area (defined as the region of the lesion within 30 μm of the luminal surface) relative to the size of the lesion, (**d**) increased ACTA2^{+} cells within the fibrous cap, (**e**) an overall decrease in the fraction of LGALS3^{+} cells, and a

large decrease in the fraction of SMC-derived LGALS3$^+$ cells (YFP$^+$LGALS3$^+$), (**f**) an increase in the ACTA2$^+$ population within the lesion, (**g**) decreased proliferation of SMC-derived cells (YFP$^+$MKI67$^+$), and (**h**) decreased overall cell death, mostly due to a decrease in SMC-derived apoptosis (YFP$^+$CASP3$^+$). *$P < 0.05$, ¥ $P = 0.07$, analysis completed by 2-way ANOVA comparing genotyping and distance from start of the BCA with a Tukey post-test, error bars are based on S.E.M. Quantification is based on analysis of five 71415 μm^2 regions in each of three sections (**d**-**g**), or two sections (**h, i**), per mouse spanning a 600μm length of the BCA. Scale bar = 50 μm. SMC YFP$^{+/+}$ *Klf4*$^{WT/WT}$*Apoe*$^{-/-}$ $n = 11$, SMC YFP$^{+/+}$ *Klf4*$^{\Delta/\Delta}$*Apoe*$^{-/-}$ $n = 8$.

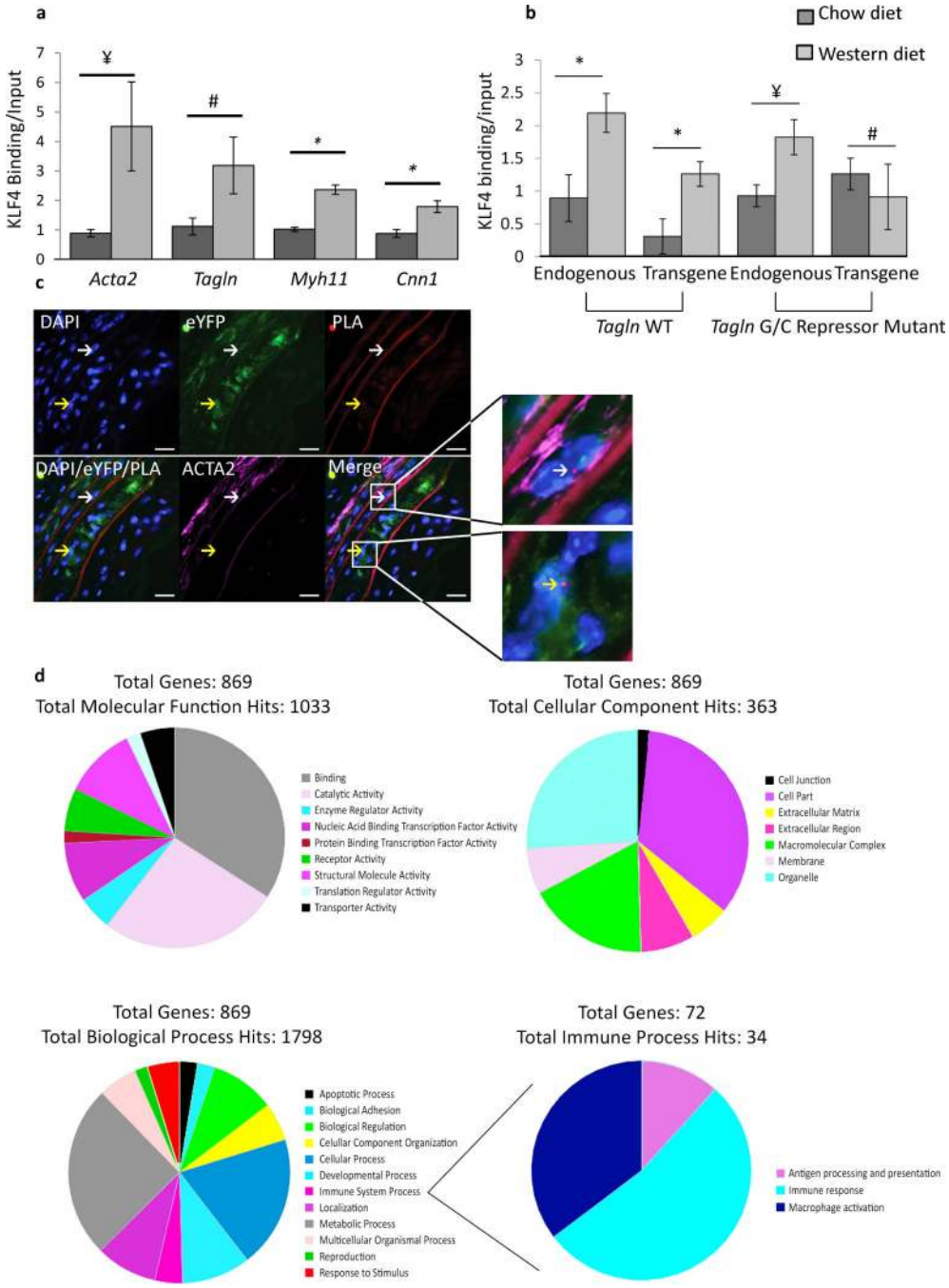

Figure 5. KLF4 binds to > 800 genes within SMC in advanced atherosclerotic lesions

(**a**) *in vivo* ChIP assays on BCAs obtained from 18 week Western diet fed *Apoe*$^{-/-}$ mice show increased binding of KLF4 to SM marker gene promoters compared to *Apoe*$^{-/-}$ mice fed a chow diet. *P*-values based on one-way ANOVA with Tukey post-test. ¥ $P = 0.07$, # $P = 0.11$, * $P < 0.05$. Error bars are based on S.E.M. (**b**) KLF4 binding to the *Tagln* promoter in response to Western diet treatment is dependent on the GC repressor element.*Apoe*$^{-/-}$ mice were crossed to either a *Tagln* wild type (WT) transgene or *Tagln* G/C repressor mutant transgene and KLF4 ChIP analyses performed on chromatin extracted from the BCA

region. *P*-values based on two-way ANOVA with Tukey post-test. ¥ $P = 0.06$, # $P = 0.43$, * $P < 0.05$. Error bars are based on S.E.M. $n = 3$ independent pooled groups of 5 mice per treatment group. (**c**) KLF4 binding to the G/C repressor element of the *Tagln* promoter *in vivo* was determined by *Klf4-Tagln* ISH-PLA. The white arrow indicates a cell where KLF4 is bound to the *Tagln* promoter of a differentiated SMC (top), while the yellow arrow identifies a phenotypically modulated SMC (bottom). Scale bar = 10 μm. (**d**) Aortic segments from the aortic root and aortic arch up to the carotid bifurcations from 18 week WD fed SMC $Klf4^{WT/WT}$ $eYFP^{+/+}$ $Apoe^{-/-}$ ($n = 14$), SMC $Klf4^{\Delta/\Delta}$ $eYFP^{+/+}$ $Apoe^{-/-}$ ($n = 14$), and 8 week old chow fed SMC $Klf4^{WT/WT}$ $eYFP^{+/+}$ $Apoe^{-/-}$ ($n = 15$) mice were utilized for ChIP-Seq analysis of KLF4 binding targets. 869 targets were enriched in Western diet treated SMC $Klf4^{WT/WT}$ $eYFP^{+/+}$ $Apoe^{-/-}$ mice as compared to SMC $Klf4^{\Delta/\Delta}$ $eYFP^{+/+}$ $Apoe^{-/-}$ mice, and thus represent putative SMC KLF4 target genes.

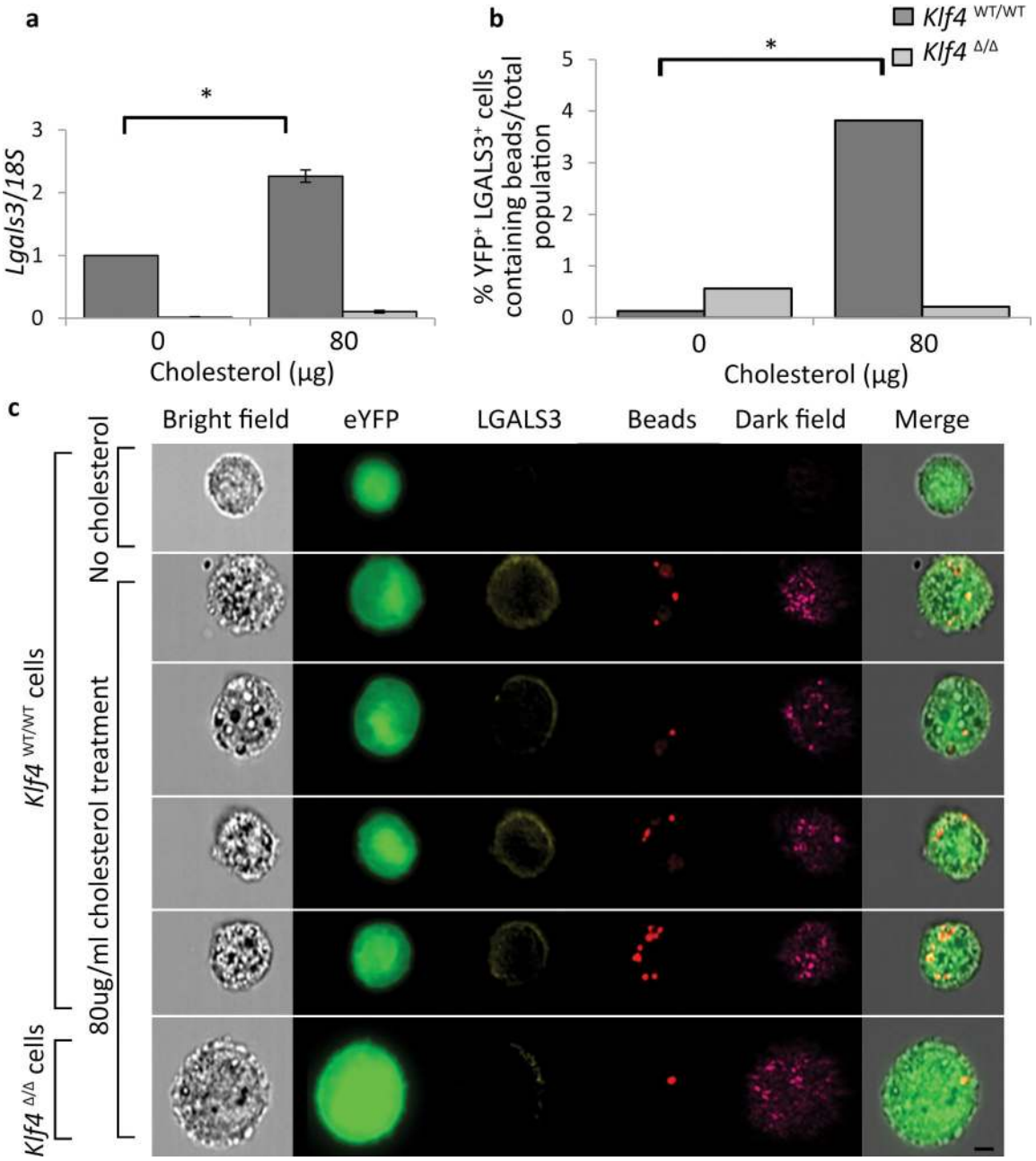

Figure 6. KLF4-dependent activation of *Lgals3*, MSC markers, and phagocytotic activity in cholesterol loaded cultured SMC

(**a**-**c**) Aortic SMCs were isolated from SMC YFP$^{+/+}$ *Klf4* $^{WT/WT}$ and SMC YFP$^{+/+}$ *Klf4*$^{\Delta/\Delta}$ mice and sorted using a FACSVantage SE DIVA to ensure a pure SMC (YFP+) cell population. (**a**) Induction of *Lgals3* mRNA expression following cholesterol loading (80 µg/mL cholesterol for 72 hours) was decreased in cells derived from SMC YFP$^{+/+}$ *Klf4*$^{\Delta/\Delta}$ as compared to cells derived from SMC YFP$^{+/+}$ *Klf4* $^{WT/WT}$ mice. *P*-values based on two-way ANOVA with Tukey post-test. *$P < 0.05$. Data normalized to *Klf4* $^{WT/WT}$ 0 ug/mL cholesterol. Error bars based on S.E.M. $n = 3$ independent experiments. (**b**-**c**) *Klf4*$^{WT/WT}$ and *Klf4*$^{\Delta/\Delta}$ cells were incubated with 0.8 µm polysterene beads for 1.5 hours after 72 hours

of cholesterol loading to induce a Mφ-like state. Cells were then analyzed on an Amnis ImagestreamX Mark II to assess expression of YFP, LGALS3, and to identify bead uptake. (**b**) Quantification of bead uptake was performed using Amnis IDEAS software. After normalization to the total population, values were subjected to Fisher's exact test, which showed that the $Klf4^{WT/WT}$ $YFP^{+}LGALS3^{+}$ cells contained significantly ($P < 0.05$) more beads than the $Klf4^{\Delta/\Delta}$ $YFP^{+}LGALS3^{+}$ cells (representative experiment from $n = 2$). (**c**) Representative images from the Amnis IDEAS software, YFP (green), LGALS3 (yellow), beads (red), Dark Field (magenta). Scale bar = 5 μm.